Natural course and classification of extensive macular atrophy with pseudodrusen-like appearance

Romano, F.; Cozzi, M.; Monteduro, D.; Oldani, M.; Boon, C.J.F.; Staurenghi, G.; Salvetti, A.P.

SDC

RETINA PODCAST

NATURAL COURSE AND CLASSIFICATION OF EXTENSIVE MACULAR ATROPHY WITH PSEUDODRUSEN-LIKE APPEARANCE

FRANCESCO ROMANO, MD,* MARIANO COZZI, MSc,* DAVIDE MONTEDURO, MD,* MARTA OLDANI, MD,* CAMIEL J. F. BOON, MD, PhD, FEBO,†‡ GIOVANNI STAURENGHI, MD, FARVO,* ANNA PAOLA SALVETTI, MD*

Purpose: To describe the imaging characteristics and topographic expansion of retinal pigment epithelium (RPE) and outer retinal atrophy in extensive macular atrophy with pseudodrusen-like appearance.

Methods: Three-year, prospective, observational study. Nine patients with extensive macular atrophy with pseudodrusen-like appearance (17 eyes; 6 women) with no other ocular conditions were annually examined; one eye was excluded because of macular neovascularization. Best-corrected visual acuity measurement, fundus photographs, blue-light autofluorescence, and optical coherence tomography were performed at each visit. Formation of atrophy was analyzed on optical coherence tomography at foveal and extrafoveal areas following the Classification of Atrophy Meeting recommendations. Spatial enlargement throughout four sectors was assessed on blue-light autofluorescence after placing an Early Treatment for Diabetic Retinopathy Study grid centered on the foveola.

Results: Mean age was 53.0 ± 2.1 years at baseline with a follow-up of 36.6 ± 0.7 months. Thinning of the outer nuclear layer and disruption of the ellipsoid zone initially appeared above areas of RPE–Bruch membrane separation and preceded RPE atrophy. Subfoveal fibrosis was seen in 65% of the eyes. Superior sector involvement was found in all patients at baseline and was significantly larger than the other sectors at any time point ($P < 0.001$). Best-corrected visual acuity declined from 68.0 ± 15.7 letters to 44.8 ± 14.9 letters during the follow-up and was significantly associated with subfoveal atrophy ($P < 0.001$) and fibrosis ($P = 0.02$).

Conclusion: Our findings suggest that primary alterations in patients with extensive macular atrophy with pseudodrusen-like appearance are present at the outer segment–RPE interface, with the superior Early Treatment for Diabetic Retinopathy Study sector being the most vulnerable, which progresses to extensive atrophy of the RPE and outer retinal layers. Accordingly, we propose a three-stage disease classification.

RETINA 43:402–411, 2023

Extensive macular atrophy with pseudodrusen-like appearance (EMAP) is a rare—albeit increasingly recognized—form of macular degeneration that affects middle-aged individuals with a slight female predominance.[1–3] Frequent symptoms include impaired dark adaptation and central vision loss, which result in an enormous burden for this working-age population, ultimately leading to legal blindness within 3 to 10 years since onset.[1,2,4]

Typical fundus findings include bilateral widespread pseudodrusen-like lesions throughout the posterior pole and retinal midperiphery, vertically oriented macular atrophy with early foveal involvement and often peripheral paving stone lesions.[1] Although the bilateral and remarkably symmetric presentation seems to suggest a genetic predisposition, EMAP pathogenesis still remains largely elusive.

To date, a systematic clinical classification and longitudinal description of the retinal alterations occurring in EMAP are missing. The rate of retinal pigment epithelial (RPE) atrophy expansion has been retrospectively assessed using blue-light autofluorescence (BAF)

and optical coherence tomography (OCT) modalities, highlighting the fast progression of the disease.[5] In this regard, recent imaging advances have emphasized the role of OCT in detecting the structural alterations occurring in the retina and the choroid as a result of the high axial resolution reached by the spectral-domain technology.[6,7] Optical coherence tomography has indeed permitted to characterize the outer retinal and RPE changes that precede the development of atrophy in many retinal diseases such as age-related macular degeneration (AMD) and other retinal dystrophies.[8–12]

The aim of our study is to describe the multimodal imaging alterations and the topographic expansion of macular atrophy in EMAP and to correlate these findings with visual function.

METHODS

The study was designed as a prospective and observational case series. The research was approved by the Institutional Review Board of Luigi Sacco Hospital (University of Milan; Milan, Italy). The procedures adhered to the tenets of the Declaration of Helsinki, and written informed consent was obtained from all the study subjects.

The primary outcome of our research was to report the longitudinal changes that lead to RPE atrophy formation in EMAP. Secondary outcomes included the evaluation of possible visual function correlations and the introduction of a novel disease classification.

Study Population

A series of patients affected by EMAP were consecutively recruited from January 2016 to June 2018. Follow-up visits were scheduled on a yearly basis (±2 months) for three consecutive years.

From the *Eye Clinic, Department of Biomedical and Clinical Science, Luigi Sacco Hospital, University of Milan, Milan, Italy; †Department of Ophthalmology, Amsterdam University Medical Centers, Amsterdam, the Netherlands; and ‡Department of Ophthalmology, Leiden University Medical Center, Leiden, the Netherlands.

M. Cozzi has the following disclosures: Bayer (recipient), Nidek (recipient). G. Staurenghi is consultant for Heidelberg Engineering, Optos, OptoVue, CenterVue, Allergan, Bayer, Genetech, Novartis, Quantel Medical, Carl Zeiss Meditec, Boheringer, Topcon, Roche. F. Romano, D. Monteduro, M. Oldani, C. J. F. Boon, and A. P. Salvetti have no financial disclosures.

Supplemental digital content is available for this article. Direct URL citations appear in the printed text and are provided in the HTML and PDF versions of this article on the journal's Web site (www.retinajournal.com).

Reprint requests: Giovanni Staurenghi, MD, FARVO, Eye Clinic, Department of Biomedical and Clinical Sciences, Luigi Sacco Hospital, University of Milan, Via G.B. Grassi 74, 20157 Milan, Italy; e-mail: giovanni.staurenghi@unimi.it

The following criteria had to be fulfilled to be included in the study: 1) funduscopic and imaging findings compatible with the diagnosis of EMAP (bilateral widespread pseudodrusen-like lesions from the posterior pole to the midperipheral retina, macular atrophy with predominant vertical axis, frequent peripheral paving stone lesions); 2) age younger than 55 years at the onset of visual symptoms (e.g., visual loss, reading disability, impaired dark adaptation); and 3) clear media and acceptable fixation. Exclusion criteria included the following: 1) any ocular or systemic condition potentially affecting our analysis; 2) family history or the identification of pathogenic mutations associated with inherited retinal dystrophies; 3) the presence at baseline or the development during the follow-ups of macular neovascularization (MNV); 4) refractive errors with spherical equivalent greater than ±6 diopter (D); 5) any past ocular surgery such as cataract or intravitreal injections; 6) the inability to complete the follow-up study. Both eyes of our participants were considered eligible for the study given the rarity of the disease.

Procedures

The patients underwent a complete ophthalmic evaluation at baseline and during the follow-up visits, including measurement of best-corrected visual acuity (BCVA) using the Early Treatment for Diabetic Retinopathy Study (ETDRS) chart; slit-lamp biomicroscopic examination; 60° field-of-view color fundus photography of posterior pole (EIDON; CenterVue, Padua, Italy); 30° × 30° and 55° × 55° BAF images (Spectralis HRA2; Heidelberg Engineering GmbH, Heidelberg, Germany); and dense 25° × 30°, 61-line OCT volume scans of macular area (Spectralis OCT2; Heidelberg Engineering GmbH).

Optical coherence tomography angiography or fluorescein and indocyanine green angiography could be performed at any time point at investigator's discretion if the occurrence of MNV was suspected. All the imaging studies were acquired by a reading center-certified staff member (M.C.).

If results of prior genetic analyses were not available, patients underwent blood testing for a genetic panel including 148 genes associated with nonsyndromic retinal dystrophies and rare complement variants through next-generation sequencing of target regions (MiSeq System, Nextera Rapid Capture method; Illumina Inc, San Diego, CA), as reported in one of our previous publications.[5]

Morphologic and Topographic Grading

All the acquired images were carefully analyzed by two ophthalmologists with experience in the field

of multimodal retinal imaging (A.P.S. and F.R.). The mean values provided by the two graders were adopted for quantitative measurements, whereas a third senior grader (G.S.) was consulted to review the obtained measures or in case of discordant qualitative findings.

The morphological alterations were longitudinally described using the OCT volume scans. Optical coherence tomography changes occurring at the foveal and extrafoveal level unaffected by RPE atrophy were reported separately. The following alterations based on the recent Classification of Atrophy Meetings were reviewed by the two graders at each visit: thinning of the outer nuclear layer, outer plexiform layer subsidence, disruption of external limiting membrane (ELM) and of ellipsoid zone (EZ), attenuation/atrophy of RPE and choroidal hypertransmission.[11,13–18] Additional pathologic findings were identified on OCT and included in our analysis: RPE–Bruch membrane (BM) separation, perifoveal and subfoveal fibrosis, and persistence of heterogeneous hyperreflective material. Macular fibrosis was defined on the base of fundus photographs and OCT scans according to the characteristics described by Souied et al.[19]

To perform a topographic mapping of macular atrophy, a modified ETDRS grid available on Heidelberg Eye Explorer (version 1.10.4.0) was centered on the foveola of the 30° × 30° infrared image coacquired with the OCT volume to better identify the center of the foveal pit. The grid was then moved to the 30° × 30° BAF image using the "copy/paste overlay" tool available on the Heidelberg software. The posterior pole was divided by the grid at baseline in a central subfield with a 1,200-μm diameter (foveal center) and four extrafoveal sectors/slices with a 7,200-μm diameter (superior, nasal, inferior, and temporal), as previously described in the literature.[20,21] Follow-up imaging studies were similarly aligned to the corresponding baseline images.

Autofluorescence images were carefully graded for the extent of atrophy and for the perilesional BAF pattern (e.g., none, focal, patchy, banded, diffuse, and diffuse trickling).[3] Atrophy of the RPE was labeled as "well-defined areas of reduced autofluorescence signal on BAF images" and manually measured for each sector using the available "free-hand" tool.[22] Simultaneous OCT evaluation was performed to rule out confounding factors able to alter the autofluorescence signal (e.g., fibrosis, macular pigment, hemorrhages). The size of RPE atrophy was expressed both as square millimeters and as percentage of the total area of each sector (9.89 mm^2) for statistical purposes.

Statistical Analysis

Statistical analyses were performed using SPSS statistics version 26.0 software (IBM Corporation, Armonk, NY) with significance being set at $P < 0.05$. The normal distribution of the studied variables was explored by means of Shapiro–Wilk test, and descriptive statistics were expressed as mean ± SD (range), median (quartiles), or frequencies (%) where appropriate.

The following variables were included in our analysis: age, sex, eye laterality, time, BCVA, total and sectorial atrophy of the RPE, outer plexiform layer subsidence, ELM and EZ disruption, RPE–BM separation, heterogeneous hyperreflective material, subfoveal RPE atrophy, and subfoveal fibrosis.

The differences among multiple subgroups at each visit were assessed by means of analysis of variance adopting Tukey honestly significant difference test for post hoc analysis, whereas one-way analysis of variance with repeated measures followed by post hoc analysis with Bonferroni correction was used for multiple within-subject comparisons over time. The effect of the clinical and imaging variables on BCVA was initially tested using univariate linear regression; only those that significantly correlated with BCVA on univariate analysis were further investigated using multiple linear regression models.

The agreement between the two independent graders was tested using intraclass correlation coefficients (95% confidence intervals) and Cohen k-factors (k, 95% confidence intervals) for quantitative and qualitative variables, respectively.

RESULTS

Overall, a total of nine patients (17 eyes) were recruited and completed the 36-months of follow-up, with a female predominance (66.7%). The mean age of our population at baseline was 53.0 ± 2.1 years (range: 50–56 years). One eye of a patient developed Type 2 MNV during the follow-up leading to poor visual outcomes (20/400 Snellen) and was therefore excluded from our analysis. The results of genetic testing did not reveal any pathogenic variants able to explain the disease phenotype.

Well-demarcated hypoautofluorescent areas of macular atrophy surrounded by a slightly hyperautofluorescent ("diffuse-trickling") background were observed in all eyes at baseline using BAF imaging. A linear and significant enlargement of atrophy was detected over time at a rate of 3.0 ± 0.9 mm^2/year ($P < 0.001$; baseline: 13.9 ± 6.1 mm^2 vs. Year-3: 22.9 ± 4.8 mm^2). Dye-based angiography was performed in

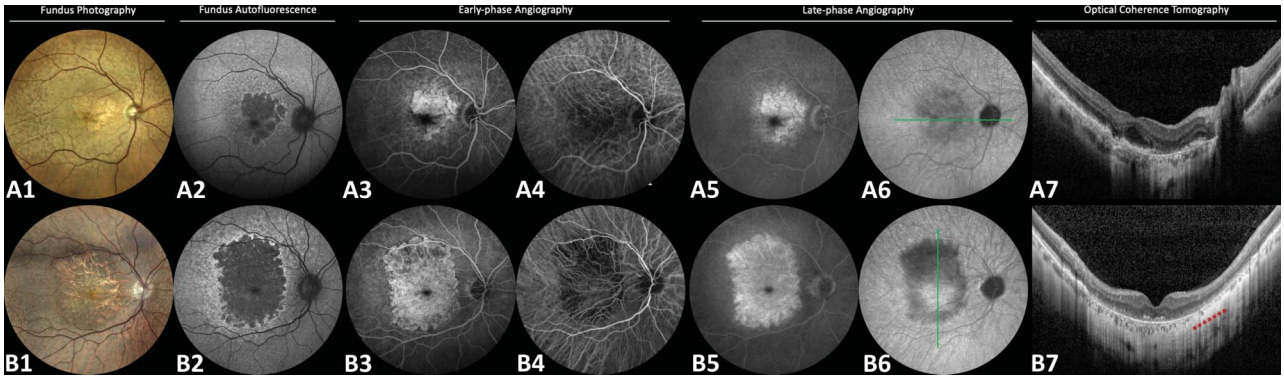

Fig. 1. Multimodal imaging findings in two patients with EMAP. In the first patient (first row, **A1**–**A7**), a well-demarcated area of macular atrophy with polycyclic margins and foveal sparing can be observed on fundus photograph and BAF. Atrophic areas are surrounded by few small "dot-like" pseudodrusen at the posterior pole and by several pseudodrusen-like lesions extending beyond the vascular arcades (**A1**). Blue-light autofluorescence image shows a slightly hyperautofluorescent ("diffuse-trickling") background at the posterior (**A2**). Increased fluorescence is noticed both in the early and late phases of fluorescein angiography in correspondence with macular atrophy as a result of window effect, whereas pseudodrusen-like lesions disclose minimal staining over time (**A3** and **A5**). Indocyanine green angiographic studies show increased visibility of the underlying choroidal vessels in the early phase and slight hypofluorescence in the late phase, whereas pseudodrusen-like lesions exert progressive masking effect over time (**A4** and **A6**). Widefield horizontal OCT (**A7**) scan highlights diffuse EZ disruption over areas of separation between the RPE and BM with RPE atrophy nasal to the fovea. In the second patient (second row, **B1**–**B7**), macular atrophy appears more extensive, has polycyclic margins, and acquires a more vertical configuration. Similar dot-like pseudodrusen and pseudodrusen-like lesions surround the atrophic area (**B1**) and the hyperautofluorescent background is maintained (**B2**). Choroidal vascular alterations become more evident in the superior macula as testified by the reduced hyperfluorescence on fluorescein angiography in the early phase (**B3**) and by the remarkable hypofluorescence on ICGA in the late phase (**B6**). Vertical widefield OCT scan confirms the significant choroidal vascular atrophy superiorly to the macula (**B7**, red asterisks). ICGA, indocyanine green angiographic.

four patients (44.4%) and showed early and late hyperfluorescence in correspondence of the atrophic areas with slight staining of the pseudodrusen-like lesions on fluorescein angiography (Figure 1, A1–B5). Early-phase indocyanine green angiography images instead documented an increased visibility of the underlying choroidal vessels in the atrophic areas (Figure 1, A1–B4), whereas a slight hypofluorescence was visible in late phases in particular in more advanced cases characterized by profound choroidal vascular atrophy (Figure 1, A1–B6).

Best-corrected visual acuity of our cohort declined linearly from baseline to the last visit (68.0 ± 15.7 letters vs. 44.8 ± 14.9 letters), with a rate of −7.7 ± 5.2 ETDRS letters/year. The complete demographic and clinical characteristics are reported in Table 1.

Structural Progression

At the foveal level, most eyes (15, 88.2%) had RPE–BM separation at baseline, whereas the remaining two eyes were already affected by subfoveal RPE atrophy (11.8%). In all cases, EZ disruption preceded the ELM alterations and the appearance of the subfoveal RPE atrophy with choroidal hypertransmission on OCT (4.3 ± 7.6 months, 21.0 ± 13.7 months, and 26.2 ± 14.0 months from baseline, respectively) (Figure 2). Subfoveal fibrosis in the absence of intraretinal/subretinal fluid was detected in 11 eyes after a mean of 17.5 ± 14.6 months of follow-up (64.7%), with fibrosis appearing in the perifoveal region and subsequently extending to the fovea in five cases (29.4%). An example of subfoveal fibrosis development is illustrated in Figure 2.

In the extrafoveal macular areas, RPE–BM separation and generalized thinning of the outer nuclear layer were observed in all patients at presentation. Retinal pigment epithelium–BM separation was accompanied by diffuse irregularity of the EZ in 10 eyes (58.8%) at baseline, whereas the remaining seven eyes developed focal EZ disruption during the follow-up (41.2%).

Table 1. Demographic and Clinical Characteristics of the Study Cohort

	Study Cohort
Patients, n (eyes)	9 (17)
Age at baseline, years (range)	53.0 ± 2.1 (50–56)
Sex, n (%)	
Males	3 (33.3)
Females	6 (66.7)
Eye laterality, n (%)	
Right	9 (52.9)
Left	8 (47.1)
Follow-up length, months (range)	36.6 ± 0.7 (36–38)
RPE atrophy, mm^2 (range)	
Baseline	13.9 ± 6.1 (0.7–23.8)
Year 1	17.1 ± 5.7 (2.1–25.2)
Year 2	20.0 ± 5.6 (4.3–28.0)
Year 3	22.9 ± 4.8 (11.1–30.0)
Subfoveal fibrosis, n (%)	11 (65)
BCVA, ETDRS letters (Snellen)	
Baseline	68.0 ± 15.7 (20/40)
Year 1	58.3 ± 22.8 (20/65)
Year 2	54.2 ± 20.5 (20/80)
Year 3	44.8 ± 15.0 (20/125)

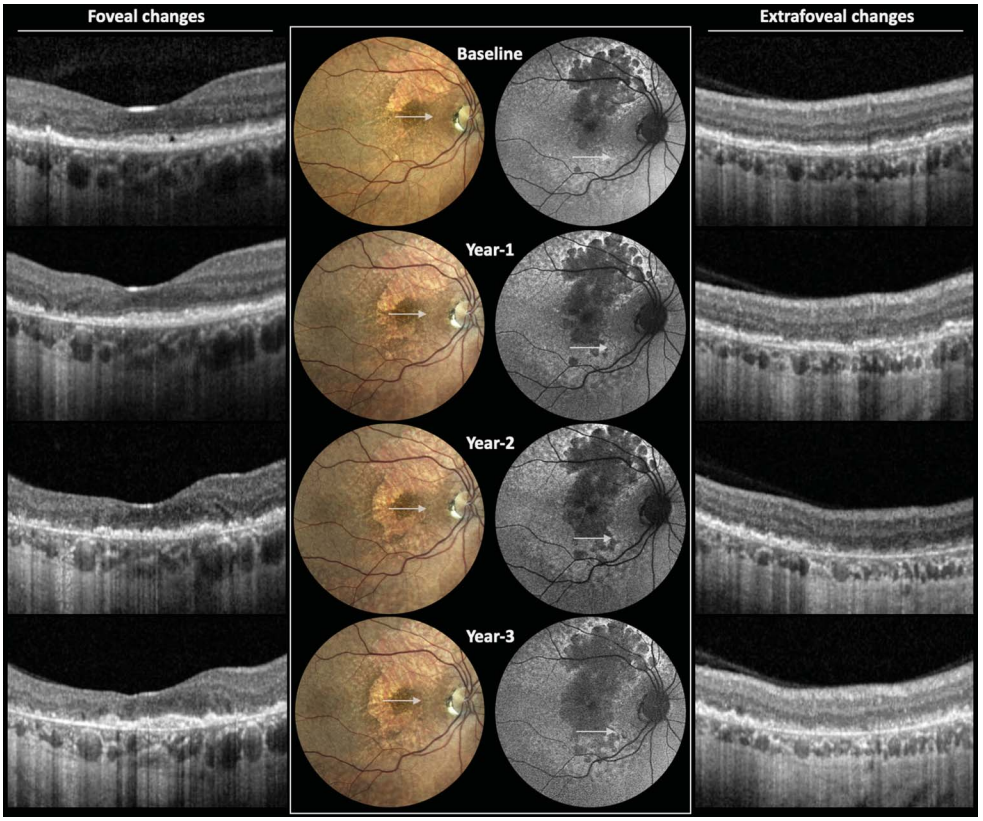

Fig. 2. Progressive foveal and extrafoveal alterations occurring in EMAP. (Left, foveal changes) Severe disruption of the EZ in the foveal area is present at baseline and progresses toward EZ disappearance at Year-2 follow-up. Conversely, disruption of the ELM and of the RPE appears later during the course of the disease (Year 2) and rapidly leads to the development of RPE atrophy with a collapse of the inner retinal layers (Year 3). At last visit, a small subfoveal fibrotic nodule becomes visible. (Right, extrafoveal changes) Significant thinning of the ONL and diffuse disruption of the EZ are observed at baseline above areas of RPE–BM separation. Focal areas of RPE atrophy progressively appear (Year 1) and coalesce over the follow-up (Years 2–3). Finally, the inner retinal layers subside, leaving a typical subretinal hyperreflective heterogeneous material (Year 3), whereas choroidal thickness accordingly thins out. ONL, outer nuclear layer.

External limiting membrane disruption typically followed the alteration of the EZ band and occurred in concomitance with the attenuation of the RPE layer. Finally, atrophy of the RPE progressively developed with a typical barcode appearance, leaving space to persistent subretinal heterogeneous hyperreflective material and to subsidence of the outer plexiform layer (Figure 3). The agreement between the two readers was considered good for all the qualitative measurements (k = 0.84; range, 0.78–0.91) (see **Supplemental Digital Content 1**, http://links.lww.com/IAE/B871).

Topographic Progression

At baseline, atrophy of the RPE was detected in the superior sector of the macula in all cases (100%), in the nasal sector in 13 eyes (76.5%), in the temporal sector in 14 eyes (82.4%), and in the inferior one in 15 eyes (88.2%). Almost all eyes (16 of 17, 94.1%) had atrophic changes in all four ETDRS sectors at their last examination, whereas one eye had the temporal sector preserved until Year 3.

The size of RPE atrophy increased significantly and linearly over time in all sectors during follow-up (all $P < 0.05$), with the exception of the superior section of the macula, which reached a plateau in growth rate between Year 2 and Year 3 ($P = 0.10$). The extent of RPE atrophy was significantly larger in the superior sector compared with the other sectors both at baseline and at each follow-up examination (all $P < 0.001$). Although the inferior sector was more extensively affected than the nasal and temporal ones, statistical significance was not reached at any time point (all $P > 0.05$). The interobserver agreement was rated excellent for the quantitative measures of atrophy (intraclass correlation coefficient = 0.904, [0.843–0.952]) (see **Supplemental Digital Content 1**, http://links.lww.com/IAE/B871). The distribution of macular atrophy in the different slices over time is plotted in Figure 4.

Visual Outcomes

Univariate analysis showed that BCVA was significantly and positively affected by the preservation of subfoveal RPE–BM separation ($P < 0.001$) and negatively by time ($P = 0.001$), size of macular atrophy ($P < 0.001$), disruption of subfoveal EZ ($P = 0.007$) and ELM ($P < 0.001$), and by the appearance of subfoveal RPE atrophy and of subfoveal fibrosis (both $P < 0.001$). When assessing the significant variables with multivariate analysis ($R^2 = 0.822$, $P < 0.001$), BCVA appeared meaningfully diminished only by the development of subfoveal atrophy of the RPE ($P < 0.001$) and by the formation of subfoveal fibrosis ($P = 0.02$).

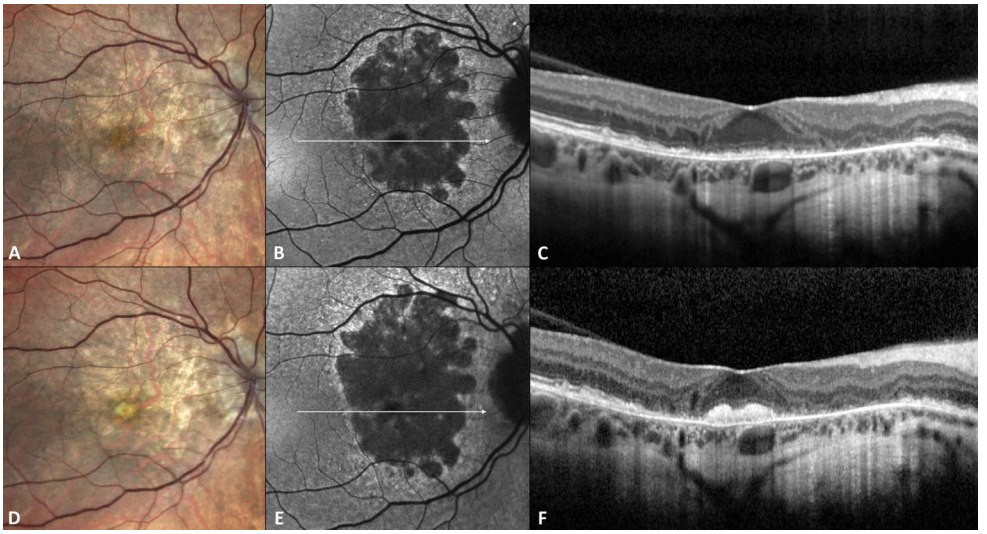

Fig. 3. Formation of subfoveal fibrosis in the right eye of a patient with EMAP. A granular reflex can be observed in the foveal area on color fundus photography at baseline (**A**) with intact foveal hypoautofluorescence (**B**) and disruption of the EZ on OCT (**C**). After 2 years of follow-up, a single nodule of subfoveal fibrosis becomes visible on color fundus photography (**D**) in the absence of remarkable subretinal/intraretinal exudation (**F**). Meaningful increment of RPE atrophy can be appreciated in extrafoveal areas on BAF (**E**).

Graphical representation of multivariate analysis is depicted in **Supplemental Digital Content 2** (http://links.lww.com/IAE/B872).

Clinical Classification

Based on our imaging findings and on visual symptoms reported by our patients, we propose a three-stage classification system of EMAP (Figure 5). Stage 1 is characterized by splitting of the RPE–BM complex with overlying focal EZ disruption at the posterior pole surrounded by diffuse pseudodrusen-like lesions that extend into the retinal midperiphery. Few discrete and nonconfluent areas of RPE atrophy can be seen in the superior macula, and visual acuity is thus well preserved.

In Stage 2, RPE atrophy becomes confluent and extensive acquiring a prevalent vertical orientation, but the fovea remains unaffected. Visual symptoms, including reading disabilities and impaired dark adaptation, become prominent, but BCVA remains relatively high.

In Stage 3, the fovea is affected by the disease and leads to significant deterioration of visual acuity. As previously mentioned, foveal involvement can occur

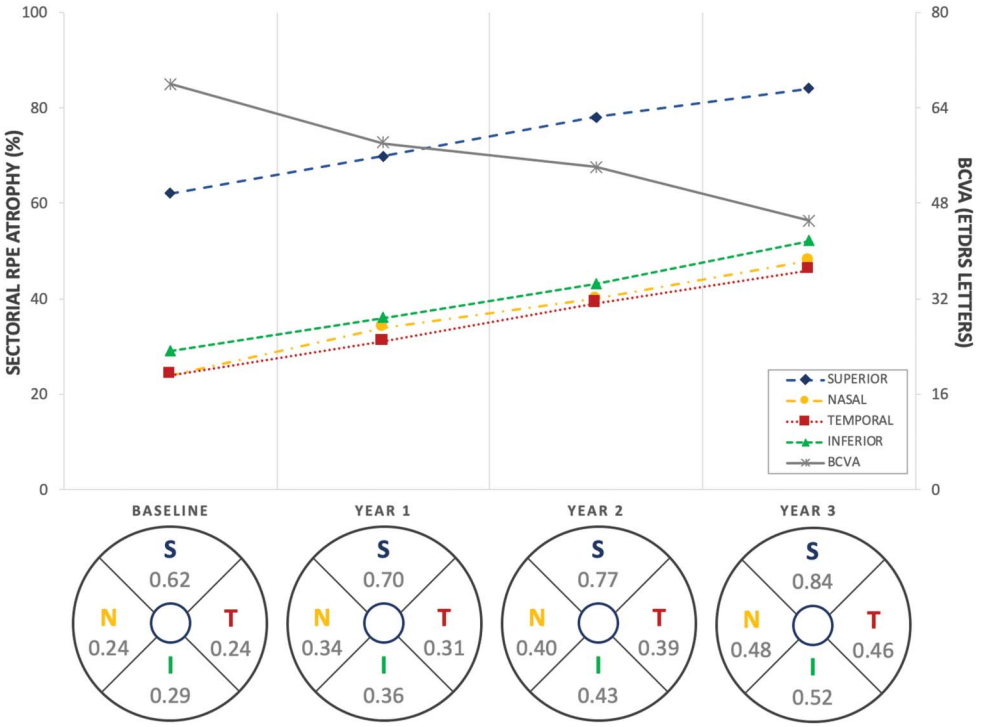

Fig. 4. Expansion of RPE atrophy in the different ETDRS sectors. Retinal pigment epithelium atrophy appears significantly larger in the superior sector (blue dotted line, 62% of the total area) at baseline compared with the other sectors and increases linearly over time until reaching a plateau between Year 2 and Year 3 (84% of the total area). Retinal pigment epithelium atrophy increases linearly also in the remaining three sectors without meaningful differences. By contrast, visual acuity progressively decreases over the follow-up (gray line). Complete data with the percentage growth of RPE atrophy in the different sectors is shown at the bottom of the graph.

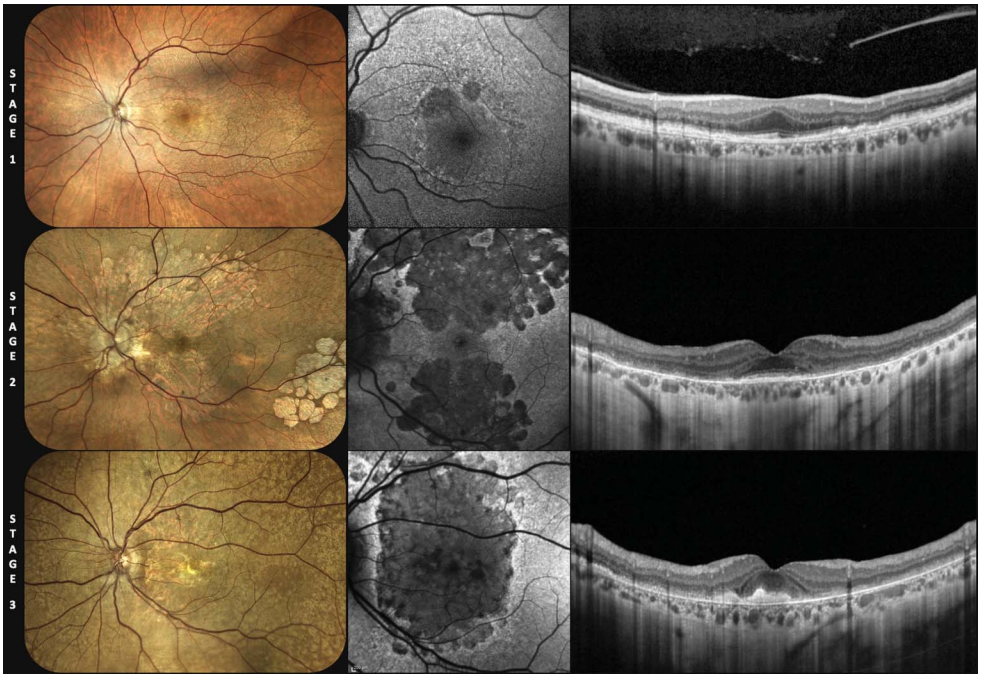

Fig. 5. Proposed classification of EMAP in three different stages. Stage 1 patients show diffuse pseudodrusen-like deposits that can be visualized as irregular RPE–BM separation with overlying disruption of the EZ. Few, nonconfluent areas of RPE atrophy can be found, generally located in the superior sector. In Stage 2, the RPE atrophy becomes larger, confluent, and extends to the other ETDRS sectors, but the foveal area remains spared. Stage 3 is instead characterized by foveal derangement, which can occur by means of RPE atrophy formation or through the development of fibrosis.

through atrophy of the RPE (Figure 3A) or through the development of subretinal fibrosis (Figure 3B). Finally, we propose to add a "+" disease feature in case of MNV development at any stage of the disease. Table 2 summarizes these findings.

Discussion

In this prospective study, we analyzed the sequence of alterations leading to macular atrophy formation in EMAP patients over 3 years of follow-up and we proposed the first classification of this condition.

Extensive macular atrophy with pseudodrusen-like appearance is an intriguing form of macular atrophy that relentlessly leads middle-aged patients to legal blindness within a decade after clinical diagnosis.[1,5] In this study, we further highlight the rapid progression of the disease, and we unveil the OCT signs that define the earliest structural changes and predict the development of macular atrophy. The morphological abnormalities observed in our cohort indicate that the first identifiable alterations occur at the level of the photoreceptors and the RPE layers. Indeed, the earliest OCT findings include significant thinning of the outer nuclear layer and RPE splitting from the BM, followed by the disruption of the hyperreflective outer retinal bands. These changes appear to precede the progression toward complete RPE and outer retinal atrophy (cRORA) with the consequent disruption of the ELM and the descent of the inner retinal layers. The superior sector is the first and most extensively affected sector by macular atrophy, contributing to the typical vertical \orientation seen

Table 2. Proposed Clinical Staging of EMAP

Stage		Multimodal Imaging findings	Symptoms
1		Widespread RPE–BM separation with focal or diffuse EZ attenuation; absent or minimal patches of RPE atrophy	Impaired dark adaptation and altered color perception
2		Appearance of several patches of RPE atrophy (predominantly in superior sector) with foveal sparing	Impaired dark adaptation, reading difficulties, mild visual loss
3		Extensive macular atrophy with foveal involvement	Severe visual loss, exophoria, and significant impact on quality of life. Ultimately, legal blindness
	A	Foveal atrophy	
	B	Subfoveal fibrosis	
+		Development of MNV	Metamorphopsias and/or sudden visual loss

in EMAP. Foveal involvement takes place later in the course of the disease and frequently manifests as subfoveal fibrosis with significant visual loss.

Since the first description by Hamel et al[1] RPE atrophy in EMAP has been described as oval shaped with a larger vertical diameter. Our quantitative assessment using the ETDRS grid provided evidence that the superior sector of the macula is the most frequently and extensively affected one at diagnosis and thus reflects the typical vertical configuration of cRORA described in EMAP.[1,2,4] The preferential superior localization of pseudodrusen-like lesions and of the initial cRORA patches reflects the behavior of geographic atrophy and is likely related to the reduced perfusion of those areas because of gravity and to the higher density of rod photoreceptors.[20,23,24] The majority of these pseudodrusen-like lesions has a "ribbon" appearance, and—differently from AMD—they are not confined to the posterior pole but homogeneously extend to the retinal midperiphery. "Dot" pseudodrusen-like lesions are instead confined to the macular region similarly to what occurs in AMD but represent a rarer finding in our patients. In this regard, we cannot exclude that the diffuse separation between the RPE and the BM may mask their presence in the late stage of the disease.[25] Macular atrophy sequentially extends from the superior macula to the other ETDRS sectors and—when uniformly implicated—acquires an oval shape. In almost half of our cases, we observed a peripapillary extension of the RPE atrophy further accentuating the vertical configuration of atrophy.

Our data describe a novel mechanism of cRORA formation that slightly differs from that observed in geographic atrophy secondary to AMD.[8–11] This distinctive pattern—characterized by extensive and homogeneous damage of photoreceptor outer segments—carries important pathogenic implications and might be used as a possible end point for future therapeutic attempts. The more extensive and earlier involvement of extrafoveal areas can be ascribed to several reasons including the faster turnover of perifoveal cones and rods, the higher vulnerability of these areas to age-related oxidative stress, and finally the possible protective role of macular pigments on the central L-/M-cones.[26–31]

In addition to AMD, several forms of early-onset atrophic macular degeneration must be differentiated from EMAP in clinical settings.[32–39] The development of diffuse RPE–BM separation has already been described in association with pseudodrusen in Sorsby fundus dystrophy, pseudoxanthoma elasticum, and late-onset retinal degeneration,[37,40] whereas a similar extension of subretinal drusenoid deposits to the retinal midperiphery has been observed in late-onset retinal degeneration and pseudoxanthoma elasticum patients, who also experience impaired dark adaptation.[25,40,41] The absence of family history for any macular degeneration, the characteristic topography of lesions, and the lack of other typical fundus alterations (e.g., flecks, soft and cuticular drusen), however, are consistent findings in EMAP patients, which allow to differentiate this form from late-onset Stargardt, Malattia Leventinese, cuticular drusen, Sorsby fundus dystrophy, late-onset retinal degeneration, and central areolar choroidal dystrophy.[32] In addition, we did not detect any other clinically significant abnormality at the systemic level, differently from what occurs in other conditions such as pseudoxanthoma elasticum and mitochondrial retinopathies.[36,39]

Although we cannot exclude that the impaired trafficking through the BM meaningfully contributes to the pathogenesis of EMAP, other clinical characteristics slightly differ from the aforementioned forms of macular degeneration. First, no pattern of inheritance or candidate gene has been identified in these patients so far; second, the decreased late-phase fluorescence observed in the former diseases is rarely present in EMAP using indocyanine green angiography and can be usually ascribed to the profound choroidal atrophy rather than to a primary choriocapillaris damage or to the masking effect of a thickened BM.[38,39] Finally, the retinal phenotype of EMAP largely favors the formation of macular atrophy rather than the neovascular complications (~15%).[42]

Our longitudinal assessment through multimodal imaging also permitted to identify subfoveal fibrosis in almost two thirds of cases. Fibrosis has already been described in EMAP patients after the development of MNV.[42] However, no signs of exudation or evidence of neovascular membrane were observed at any time in the current patient cohort using dye or OCT angiography. We hypothesize that a profibrotic environment might be induced by the inflammatory insult secondary to massive photoreceptor loss or by the accumulation of toxic materials at the level of the RPE, similarly to what occurs in Sorsby fundus dystrophy.[38,43] Another possible explanation may be related to minor ocular trauma that lead to the liberation of abnormal lipofuscin amounts and to a consequent fibro–glial reaction; a similar phenomenon has indeed been described as a nonspecific inflammatory process in other macular dystrophies.[44–46]

Finally, we propose the first clinical classification of EMAP that takes into consideration the most relevant multimodal imaging findings and visual symptoms referred by our patients (Table 2 and Figure 5). In summary, widespread pseudodrusen-like lesions,

diffuse RPE–BM separation, and EZ alterations represent the hallmark of the disease and deserve extensive study to gain better insight on EMAP pathogenesis (Stage 1). The significant scotomas in their central visual field and the impaired dark adaptation because of massive expansion of RPE atrophy (Stage 2) lead patients to seek the retina specialist's advice. Finally, severe and rapid central visual loss takes place when the fovea is affected by atrophy (Figure 3A), fibrosis (Figure 3B), or MNV development ("+" feature; Figure 5).

Our study is limited by the small sample size of our cohort, a problem that is inherent to all rare diseases. Other potential limitations include that lack of longitudinal functional data—for example, coming from electroretinography or microperimetry—and of a thorough assessment of choriocapillaris status contributing to EMAP pathogenesis. However, the current reliability of quantitative analysis of choriocapillaris using OCT angiography remains subject of debate, especially over areas of retinal tissue loss.[47] Furthermore, the measurement of macular atrophy in the different sectors was performed manually because the semiautomated software RegionFinder does not allow to position the ETDRS grid. The qualitative findings were instead independently evaluated by two ophthalmologists with experience in the field of retinal imaging; as demonstrated by the latest report of the Classification of Atrophy Meeting, a moderate-to-substantial agreement can be achieved after formal training to recognize the early atrophy changes.[13] Finally, we acknowledge that the proposed classification system should be considered as a starting point for better disease characterization. Indeed, knowledge regarding the early retinal and functional alterations occurring in the initial stage of EMAP is currently limited in the literature and deserves further in-depth studies.[48]

In conclusion, our study prospectively investigated the structural and spatial progression of RPE atrophy in EMAP patients. Based on our extensive analyses, we propose the first disease classification. The early EZ alterations and RPE–BM splitting seem to suggest diffuse photoreceptor injury that may primarily cause the disease or be secondary to the impaired trafficking across the RPE–BM complex. In addition, some components of the inflammatory or complement cascade may be involved in the pathogenesis of EMAP as testified by the high rate of subfoveal fibrosis in its late stage. The extensive involvement of the superior macular sector reflects the higher vulnerability of this anatomic location, as previously demonstrated for AMD.[20] Further studies are needed to corroborate our findings by means of a thorough functional assessment (e.g., microperimetry, contrast sensitivity and dark adaptometry), to gain better insight into the pathogenesis of EMAP and to identify potential future targets and end points for the treatment of this relatively early-onset, rapidly progressing disease.

Key words: extensive macular atrophy with pseudodrusen-like appearance, extensive macular atrophy with pseudodrusen-like appearance, progression, topographic, multimodal imaging, fibrosis, fundus autofluorescence, optical coherence tomography, classification.

References

1. Hamel CP, Meunier I, Arndt C, et al. Extensive macular atrophy with pseudodrusen-like appearance: a new clinical entity. Acta Ophthalmol 2009;147:609–20.
2. Douillard A, Picot MC, Delcourt C, et al. Clinical characteristics and risk factors of extensive macular atrophy with pseudodrusen: the EMAP case-control national clinical trial. Ophthalmology 2016;123:1865–1873.
3. Fleckenstein M, Mitchell P, Freund KB, et al. The progression of geographic atrophy secondary to age-related macular degeneration. Ophthalmology 2018;125:369–390.
4. Douillard A, Picot MC, Delcourt C, et al. Dietary, environmental, and genetic risk factors of Extensive Macular Atrophy with Pseudodrusen, a severe bilateral macular atrophy of middle-aged patients. Sci Rep 2018;8:6840.
5. Romano F, Airaldi M, Cozzi M, et al. Progression of atrophy and visual outcomes in extensive macular atrophy with pseudodrusen-like appearance. Ophthalmol Sci 2021;1:100016.
6. Khanifar AA, Koreishi AF, Izatt JA, Toth CA. Drusen ultrastructure imaging with spectral domain optical coherence tomography in age-related macular degeneration. Ophthalmology 2008;115:1883–1890.
7. Schuman SG, Koreishi AF, Farsiu S, et al. Photoreceptor layer thinning over drusen in eyes with age-related macular degeneration imaged in vivo with spectral-domain optical coherence tomography. Ophthalmology 2009;116:488–496.e2.
8. Fleckenstein M, Issa PC, Helb HM, et al. High-resolution spectral domain-OCT imaging in geographic atrophy associated with age-related macular degeneration. Invest Ophthalmol Vis Sci 2008;49:4137–4144.
9. Yehoshua Z, Rosenfeld PJ, Gregori G, et al. Progression of geographic atrophy in age-related macular degeneration imaged with spectral domain optical coherence tomography. Ophthalmology 2011;118:679–686.
10. Schaal KB, Gregori G, Rosenfeld PJ. En face optical coherence tomography imaging for the detection of nascent geographic atrophy. Am J Ophthalmol 2017;174:145–154.
11. Sadda SR, Guymer R, Holz FG, et al. Consensus definition for atrophy associated with age-related macular degeneration on OCT: classification of atrophy report 3. Ophthalmology 2018; 125:537–548.
12. Rahman N, Georgiou M, Khan KN, Michaelides M. Macular dystrophies: clinical and imaging features, molecular genetics and therapeutic options. Br J Ophthalmol 2020;104:451–460.
13. Wu Z, Pfau M, Blodi BA, et al. OCT signs of early atrophy in age-related macular degeneration: interreader agreement. Ophthalmol Retina 2022;6:4–14.
14. Wu Z, Luu CD, Ayton LN, et al. Optical coherence tomography-defined changes preceding the development of drusen-associated atrophy in age-related macular degeneration. Ophthalmology 2014;121:2415–2422.

15. Ferrara D, Silver RE, Louzada RN, et al. Optical coherence tomography features preceding the onset of advanced age-related macular degeneration. Invest Ophthalmol Vis Sci 2017;58:3519–3529.
16. Thiele S, Pfau M, Larsen PP, et al. Multimodal imaging patterns for development of central atrophy secondary to age-related macular degeneration. Invest Ophthalmol Vis Sci 2018;59:AMD1–AMD11.
17. Guymer RH, Rosenfeld PJ, Curcio CA, et al. Incomplete retinal pigment epithelial and outer retinal atrophy in age-related macular degeneration: classification of atrophy meeting report 4. Ophthalmology 2020;127:394–409.
18. Wu Z, Luu CD, Hodgson LAB, et al. Prospective longitudinal evaluation of nascent geographic atrophy in age-related macular degeneration. Ophthalmol Retina 2020;4:568–575.
19. Souied EH, Addou-Regnard M, Ohayon A, et al. Spectral-domain optical coherence tomography analysis of fibrotic lesions in neovascular age-related macular degeneration. Am J Ophthalmol 2020;214:151–171.
20. Mauschitz MM, Fonseca S, Chang P, et al. Topography of geographic atrophy in age-related macular degeneration. Invest Ophthalmol Vis Sci 2012;53:4932–4939.
21. Steinberg JS, Fleckenstein M, Holz FG, Schmitz-Valckenberg S. Foveal sparing of reticular drusen in eyes with early and intermediate age-related macular degeneration. Invest Ophthalmol Vis Sci 2015;56:4267–4274.
22. Holz FG, Bindewald-Wittich A, Fleckenstein M, et al. Progression of geographic atrophy and impact of fundus autofluorescence patterns in age-related macular degeneration. Am J Ophthalmol 2007;143:463–472.
23. Spaide RF, Ooto S, Curcio CA. Subretinal drusenoid deposits AKA pseudodrusen. Surv Ophthalmol 2018;63:782–815.
24. Curcio CA, Sloan KR, Kalina RE, Hendrickson AE. Human photoreceptor topography. J Comp Neurol 1990;292:497–523.
25. Soumplis V, Sergouniotis PI, Robson AG, et al. Phenotypic findings in C1QTNF5 retinopathy (late-onset retinal degeneration). Acta Ophthalmol 2013;91:e191–e195.
26. Chen C, Wu L, Wu D, et al. The local cone and rod system function in early age-related macular degeneration. Doc Ophthalmol 2004;109:1–8.
27. Curcio CA. Photoreceptor topography in ageing and age-related maculopathy. Eye (Lond) 2001;15:376–383.
28. Curcio CA, Millican CL, Allen KA, Kalina RE. Aging of the human photoreceptor mosaic: evidence for selective vulnerability of rods in central retina. Invest Ophthalmol Vis Sci 1993;34:3278–3296.
29. Jackson GR, Owsley C, Curcio CA. Photoreceptor degeneration and dysfunction in aging and age-related maculopathy. Ageing Res Rev 2002;1:381–396.
30. Beatty S, Murray IJ, Henson DB, et al. Macular pigment and risk for age-related macular degeneration in subjects from a Northern European population. Invest Ophthalmol Vis Sci 2001;42:439–446.
31. Wang JS, Kefalov VJ. The cone-specific visual cycle. Prog Retin Eye Res 2011;30:115–128.
32. Saksens NTM, Fleckenstein M, Schmitz-Valckenberg S, et al. Macular dystrophies mimicking age-related macular degeneration. Prog Retin Eye Res 2014;39:23–57.
33. Westeneng-van Haaften SC, Boon CJF, Cremers FPM, et al. Clinical and genetic characteristics of late-onset Stargardt's disease. Ophthalmology 2012;119:1199–1210.
34. Boon CJF, Klevering BJ, Hoyng CB, et al. Basal laminar drusen caused by compound heterozygous variants in the CFH gene. Am J Hum Genet 2008;82:516–523.
35. Boon CJF, Klevering BJ, Cremers FPM, et al. Central areolar choroidal dystrophy. Ophthalmology 2008;116:771–782.e1.
36. de Laat P, Smeitink JAM, Janssen MCH, et al. Mitochondrial retinal dystrophy associated with the m.3243A>G mutation. Ophthalmology 2013;120:2684–2696.
37. Khan KN, Borooah S, Lando L, et al. Quantifying the separation between the retinal pigment epithelium and Bruch's membrane using optical coherence tomography in patients with inherited macular degeneration. Transl Vis Sci Technol 2020;9:26.
38. Sivaprasad S, Webster AR, Egan CA, et al. Clinical course and treatment outcomes of Sorsby fundus dystrophy. Am J Ophthalmol 2008;146:228–234.
39. Issa PC, Finger RP, Götting C, et al. Centrifugal fundus abnormalities in pseudoxanthoma elasticum. Ophthalmology 2010;117:1406–1414.
40. Gliem M, Hendig D, Finger RP, et al. Reticular pseudodrusen associated with a diseased bruch membrane in pseudoxanthoma elasticum. JAMA Ophthalmol 2015;133:581–588.
41. Hess K, Gliem M, Birtel J, et al. Impaired dark adaptation associated with a diseased bruch membrane in pseudoxanthoma elasticum. Retina 2020;40:1988–1995.
42. Kamami-Levy C, Querques G, Rostaqui O, et al. Choroidal neovascularization associated with extensive macular atrophy with pseudodrusen-like appearance. J Fr Ophtalmol 2014;37:780–786.
43. Sene A, Apte RS. Inflammation-induced photoreceptor cell death. Adv Exp Med Biol 2018;1074:203–208.
44. De Laey JJ, Verougstraete C. Hyperlipofuscinosis and subretinal fibrosis in Stargardt's disease. Retina 1995;15:399–406.
45. Parodi MB. Progressive subretinal fibrosis in fundus flavimaculatus. Acta Ophthalmol (Copenh) 2009;72:260–264.
46. Battaglia Parodi M, Iacono P, Romano F, Bandello F. Spectral domain optical coherence tomography features in different stages of best vitelliform macular dystrophy. Retina 2018;38:1041–1046.
47. Chu Z, Zhang Q, Gregori G, et al. Guidelines for imaging the choriocapillaris using OCT angiography. Am J Ophthalmol 2021;222:92–101.
48. Fragiotta S, Parravano M, Sacconi R, et al. A common finding in foveal-sparing extensive macular atrophy with pseudodrusen implicates basal laminar deposits. Retina 2022;42:1319–1329.